CRISPR-Cas9 Extracellular Vesicles for Treating Hearing Loss

Xiaoshu Pan[#1], Peixin Huang[#2], Samantha Ali[1], Tarun E Hutchinson[1], Nina Erwin[1], Zachary Greenberg[1], Zuo Ding[1], Yanjun Li[3], Natalia Fernadez[1], Hinrich Staecker[2]*, Mei He[1]*

[1]College of Pharmacy, Department of Pharmaceutics, University of Florida, Gainesville, Florida 32611, United States

[2]Department of Otolaryngology, Head and Neck Surgery, University of Kansas School of Medicine, Kansas City, Kansas 66160, United States

[3]College of Pharmacy, Department of Medicinal Chemistry, University of Florida, Gainesville, Florida 32611, United States

Contribute equally
*Corresponding Author: mhe@cop.ufl.edu

Abstract: The treatment of inner ear disorders remains challenging due to the intrinsic anatomical barriers. The majority treatments and delivery approaches for accessing inner hair cells are still engaged with surgical intervention, which is highly invasive and inconsistent in terms of efficacy and safety. In order to address this challenge for crossing anatomical barriers, we report an extracellular vesicle (EVs) -based delivery approach to inner hair cells, which enables carrying CRISPR/Cas9 ribonucleoprotein (RNP)-sgRNA complex in high-throughput and high efficiency. The novel Microfluidic Droplet-based Electroporation System (μDES) is developed to efficiently load cargos into EVs via millisecond pulsed, low-voltage electroporation within flow-through droplets as enormous bioreactors in a continuous-flow and scalable manner. The observed loading efficiency of CRISPR/Cas9 RNA complex into EVs (RNP-EVs) is 10-fold higher than current bulk cuvette electroporation with hundred-fold increase of processing throughput. The low-voltage electroporation minimized the Joule heating influence on nanosized EVs, which retained the native surface membrane properties of cargo-loaded EVs. Both ex vivo and in vivo testing in Shaker-1 mice model demonstrated the high biocompatibility and biodistribution of produced RNP-EVs in the mouse cochlea penetrating inner hair cells. In contrast, the CRISPR/Cas9 RNP lipid-like nanoparticles (RNP-LNPs) control group was unable to penetrate anatomical barriers to access inner hair cells. In the Shaker-1 mouse model, μDES produced RNP-EVs demonstrated much higher editing efficiency at *Myo7a*^{sh1} mRNA level and showed significant hearing recovery in the *Myo7a*$^{WT/Sh1}$ mice via Auditory Brainstem Response (ABR) testing. The report work will present a new solution to advance gene therapy in treating sensorineural hearing loss .

INTRODUCTION

Hearing loss is one of the most common neurodegenerative disorders with genetic causes in human affecting more than 450 million people worldwide[1-2]. In situ delivery of functional gene materials to cochlear hair cells is one of the most promising strategies to repair hair cells and restore hearing function *in vivo*[1, 3-6]. To date, the gene

therapy targeting cochlear hair cells are heavily relied on engineered AAV vectors that can transduce inner hair cells more efficiently. However, a few biosafety investigations of high dose AAV vectors in non-human primates are limiting the clinical translation[5, 7]. On the other hand, the commonly used AAVs in gene therapy have limited capacity on cargo size (~ ≤ 5Kb), which is unable to carry CRISPR SpCas9- gRNAs, as well as the *Myo7a* gene (∼100 Mb or a cDNA of ~ 7 Kb) we studied in this work as a hearing loss causative gene in inner ear hair cells[8]. Although the lentiviruses have a cargo capacity of ∼10 Kb, the risk of insertional mutagenesis and severe immunogenicity are still significant concerns for clinical translation[9]. Alternatively, extracellular vesicle (EVs)-based delivery is emerging as a novel, safe approach for addressing such challenges employed in gene delivery[10-13], owing to the intrinsic biocompatibility, low immunogenicity, tissue penetration ability, and superb tunability[14-17]. Although, EVs have been utilized to deliver various genes into tissues, the delivery of CRISPR/Cas9 ribonucleoprotein (RNP)-sgRNA complex has not been explored for inner ear tissue yet. The first-in-human trial using umbilical cord mesenchymal stromal cell derived EVs demonstrated their regenerative potential to attenuate inflammation-based side effects from cochlear implantation and noise trauma[10, 18], which indicates natural distribution of EVs across anatomical barriers in cochlear may present, making EVs more favorable in hearing loss gene therapy than its counterparts, viral vectors.

However, loading CRISPR RNP complex into EVs has been a grand challenge. Current methods suffer from low loading efficiency and not scalable. For instance, chemical transfection rate for CRISPR RNP complex is generally below < 25%, and the produced EVs are in low stability[19]. Utilizing cells engineered as the primary EV producer is limited with cargo type and copy numbers that can be passed to EVs for encapsulation. Although electro-transfection is more efficient in terms of transfection rate (~ 50%), the scalability is limited with only a few milliliters of processing volume in their throughput[20-21]. Different from cells, EVs generally have much smaller size and higher Brownian motion. Therefore, we introduce a novel continuous-flow platform utilizing microfluidic droplet-based EV electroporation (μDES), which can handle variable cargos loaded into EVs in large throughput and high efficiency. The saturated cargo concentration in the confined uniform droplet bioreactors can maximize mass transport and electroporation efficiency. Such streamlined EV electro-transfection using continuous-flow droplets as the enormous micro-bioreactors has not been explored elsewhere. Compared to microfluidic nanoporation for EV transfection[15, 17, 22-24], the continuous flow enables much larger scale and throughput processing (up to litter range). Only a low-voltage (~10-30 volts) DC power is needed, which avoids Joule heating and thermal damage on nanosized EVs[25]. Compared to chemical transfection which introduces unpurifiable chemicals potentially toxic to *in vivo* system, the instant electric field application across flow-through droplets in millisecond (~ms) minimizes perturbation of EV molecular components to retain the natural EV property and biocompatibility. We also employed FDA approved additive trehalose [26-30] in the buffer system to preserve EVs in good stability[29, 31], and minimize membrane aggregation[26-27] and leakage after electro-transfection as reported by other research[28], which is suited in clinical settings.

In the realm of hearing loss, CRISPR/Cas9 technology are demonstrating promising editing specificity and efficiency by targeting and correcting genetic mutations responsible for various hereditary hearing disorders[32]. For instance, it can address mutations in *TMC1*^{Bth} crucial for the development of sensory hair cells or cochlear function, potentially restoring auditory function[33]. More pioneer investigations exhibited that CRISPR/Cas9 technology can be applied to both congenital and acquired hearing loss, offering a multifaceted approach to treatment[3, 7, 33-35]. In this work, we target on *Myo7a* gene which plays an essential role in the development and maintenance of auditory hair cells. *Myo7a* mutation has been identified as the major causative gene (39–55% of the total cases) in Usher syndrome (USH1B), syndromic and non-syndromic hearing loss (DFNA11 and DFNB2), and age-related hearing loss[36-37]. Thus, timely removal of mutant myoVIIa allele could prevent progression of hearing loss. However, current *Myo7a* gene therapy is unattainable, due to limited options of vectors. Our work on both ex vivo and in vivo testing in Shaker-1 mouse model demonstrated the high biocompatibility and biodistribution in the inner ear tissue from our μDES produced RNP-EVs in mouse cochlea penetrating into inner hair cells. The RNP-EVs displayed much higher editing efficiency at *Myo7a*^{sh1} mRNA level and showed significant hearing recovery in *Myo7a* $^{WT/Sh1}$ mice via Auditory Brainstem Response (ABR) testing. In contrast, the CRISPR/Cas9 RNP lipid-like nanoparticles (RNP-LNPs) control group was unable to penetrate anatomical barriers to access inner hair cells. Our approach will allow the rapid loading of CRISPR into EVs for delivery of Cas9 without using a split vector, which offers the opportunity to customize sgRNAs addressing different mutant alleles within one gene, and enable customization to patient genetic heterogeneous mutation background, leading to a clinically translatable approach for overcoming current challenges in gene therapy.

RESULTS

High throughput and highly efficient EV electro-transfection via μDES platform

We developed μDES platform for enhancing EV transfection efficiency, loading capacity, and throughput. The concept of μDES platform and functionality are illustrated in Figure 1 A-E. The device composed one aqueous inlet with purified EVs and RNP cargos, one oil inlet, electroporation chamber and one droplet outlets which streamlines droplet generation with electroporation using a low voltage DC power supply. The device fabrication was detailed in supplemental materials. Continuous generation of droplets uniformly as enormous bioreactors in fast speed enables large-scale encapsulation of EVs with high concentration cargos (Figure 1F). In droplet space, the cargo transport under electric field is more efficient to cross transient pores from EV membrane via electrical mobility of cargo themselves, electric flux, and concentration gradient, which only needs milliseconds to complete in such small scale, in turn, maximizing the loading efficiency and capacity (Figure 1B). The uniform electric field distribution can be formed across each flow-through droplet for highly efficient electroporation as proved by COMSOL simulation in Figure 1C. Notwithstanding, droplet-based electroporation could also lower the dispersity of electric field in the small volume and contribute to more homogeneous electric distribution in small

volume range[38-40]. The COMSOL simulation of μDES device was conducted which showed uniform distribution of both flow profile and electric field profile with focusing on the droplet passing through the electroporation chamber (Figure 1 D and E). The scalability of μDES was also studied by collecting droplets in a large container (Figure 1F) with uniform size of produced droplets (Figure 1G). By using fluorescently tagged 100nm polystyrene beads as the reference particles comparable in size to EVs, it showed that good encapsulation of fluorescent signal from beads in the droplets without any significant signal outside the droplets (Figure 1H). To perform the emulsion of water-in-oil, fluorinated oil FC40 and associated fluoroSurfactant was employed to generate oil phase due to their low conductivity, chemical inertness and stability, and easy removal. Pharmaceutical grade FC40 oil is considered as the highly biocompatible and low-cost recipe for droplet generation employed in pharmaceutics and in compliance with FDA [41-42]. We also introduced the pharmaceutical grade trehalose as stabilization additive in the buffer during the electro-transfection, which can enhance the EV stability to minimize membrane fusion and leakage, in turn, improve the electro-transfection efficiency as documented in literatures[26-30, 43]. The droplet size which determines the throughput can be controlled by adjusting the pressure/flow rate of water-to-oil ratio[44]. For achieving high throughput, the droplets can be generated in high speed (~700 droplets/min), which leads to ~30 mL per hr processing throughput for each device. Note that current cuvette electroporation only handles ~100 μL per device. The electroporation power did not alter the droplet size and quantity (Figure 1 I and J). For the efficient purification of cargo-loaded EVs from excessive Cas9 cargos, we employed Ni Sepharose high performance magnetic beads to selectively capture the His-tagged Cas9 proteins. The cargo loaded EVs in aqueous phase can be collected via centrifugation through phase separation to fully remove oil phase (Figure 1A cargo-loaded EV collection).

Our platform can produce ~80% transfection rate for large proteins including CRISPR Cas9/sgRNA RNP complex, which showed significantly higher efficiency than other conventional transfection methods including direct incubation, lipofection, and cuvette electro-transfection (Figure 1K). EGFP-Cas9 were pre-assembled with gRNA at 1: 2 molar ratio before the electroporation. EVs derived from HEI-OC1 cell, a putative progenitor hair cell line, were isolated and quantified for mixing with EGFP-CRISPR/Cas9 ribonucleoprotein (RNP) in electroporation low conductivity buffer. The final concentration of 10^{10} /mL of EVs was used for Neon cuvette electroporation as the control group, and our μDES system, as well as other chemical transfection methods. The findings revealed significantly enhanced cargo loading within EVs using μDES system, with a percentage as high as 80% for EGFP and 70% for EGFP-Cas9/sgRNA, surpassing cuvette electroporation and chemical transfection methods while maintaining minimal sample loss (Figure 1K). We also compared the recovery rate with conventional cuvette electro-transfection (Figure 1L), which showed better recovery due to continuous-flow harvesting. We quantified the RNP Cas9 protein loading amount (Figure 1M) to compare between different transfection methods, the μDES group exhibited more than 10-fold increase than other methods. The reproducibility of μDES loading was characterized using qPCR to quantify sgRNA loading amount from 8

replicates, with native EVs and µDES conditioned EVs without RNPs as control groups. Results demonstrated the good loading capacity and reproducibility, and no leakage or changes from intrinsic EV molecular components (Figure 1N). Overall, the µDES platform demonstrated the advanced performance on EV cargo loading.

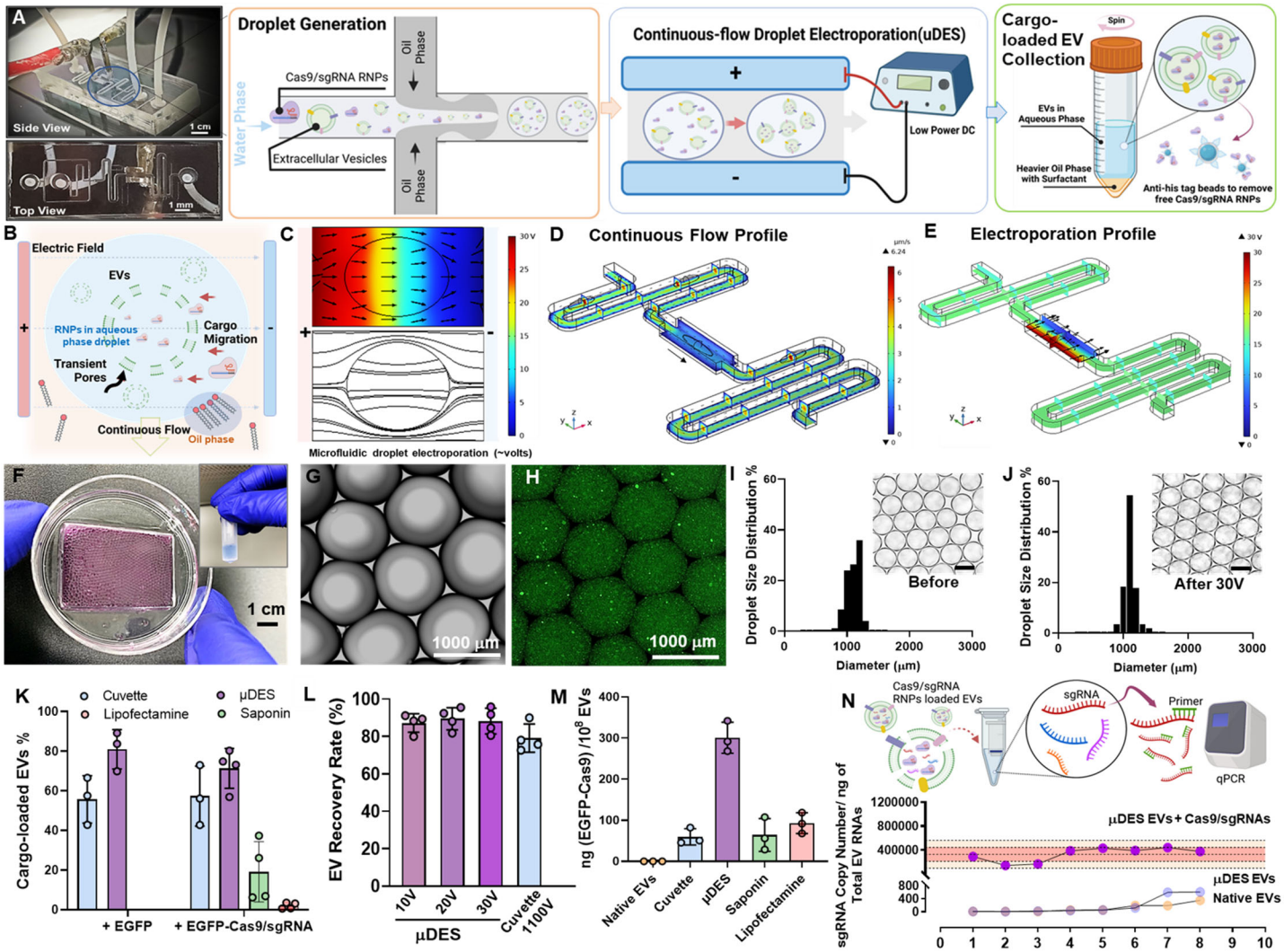

Figure 1. **(A)** Image of µDES device with illustration of continuous-flow droplet generation, droplet-based electroporation, and cargo-loaded EV harvesting and purification. **(B)** Schematic illustration of droplet-based electroporation of EVs under uniform electric field distribution as demonstrated by COMSOL simulation **(C)**. The COMSOL simulation of continuous fluidic profile **(D)** and electric field profile **(E)** to show the uniformity for precision control. **(F)** Picture of large-scale collection of cargo loaded EVs in droplets. **(G)** Microscopic image of continuous flow generated droplets with green fluorescence stained nanobeads mimicking EVs encapsulated inside **(H)**. The droplet size is uniform before**(I)** and after **(J)**electric field application for transfection (30 V). The insert scale bar is 1000 µm. **(K)** Evaluation of EV cargo loading rates among different transfection methods using fluorescence nanoparticle tracking analysis (FNTA). **(L)** EV recovery rate evaluated by NTA compared with conventional cuvette electro-transfection which requires 1100 volts for electroporation. **(M)** Quantitative measurement of CRISPR Cas9 proteins from transfected EVs normalized by EV particle number among different transfection methods. **(N)** The quantitative PCR analysis of transfected sgRNA copy number normalized by total EV RNAs. The electro-transfection was done by using µDES platform in 8 replicates. The native EVs and µDES prepared EVs without RNP cargo both served as the negative control groups. EVs are purified from HEI-OC1 ear hair cell culture.

Characterization of produced RNP EVs in high biocompatibility and tissue penetration

The μDES platform maintained a consistent flow rate, uniform electroporation pulse periods for each droplet and efficient cargo loading into EVs, therefore, retaining good EV properties as their natural un-treated EVs in terms of size (Figure 2A), zeta potential (Figure 2B), protein contents (Figure 2C), morphology and surface properties (Figure 2D). Results also indicated that μDES droplet oil phase with surfactant do not impose adverse influence on the produced EVs in aqueous phase due to phase separation. We tested the essential protein contents (CD81, TSG101, Alix) from μDES produced EVs, which is in line with native EVs in terms of expression level but carry significant amount of transfected Cas9 proteins (Figure 2C). The immune gold nanoparticle (AuNP) staining TEM imaging showed unnoticeable surface adsorption of Cas9/sgRNA RNPs from μDES produced EVs as compared with native EVs, which indicates RNA cargoes are loaded inside of EVs. By comparing with LNPs, we tested the cell biocompatibility (Figure 2E) and cellular uptake behavior (Figure 2F) via dosing HEI-OC1 ear hair cells with both μDES produced bone marrow mesenchymal stem cell derived EVs (RNP MSC-EVs) and HEI-OC1 hair cell derived EVs (RNP HEI-OC1 EVs). Both EV groups showed enhanced ability to promote ear hair cell growth compared with LNP group (LNP-102). The μDES produced RNP EVs did not show noticeable differences with their un-loaded native EVs. After one-hour cellular uptake, μDES produced EGFP-fused Cas9/sgRNA RNP MSC EVs exhibited higher uptake rate for cytoplasmic release and gradual entry into the nucleus (white arrow indication) compared with LNP group (Figure 2F). In order to further characterize the *in vivo* ear tissue biodistribution behavior, three groups of RNP*^{EGFP} LNP, μDES produced RNP*^{EGFP} MSC EVs and RNP*^{EGFP} HEI-OC1 EVs were used via posterior semicircular canal injection into Shaker-1 mice ear individually. The confocal imaging from LNP group showed the ineffective distribution for entering into inner ear hair cells (Figure 2G and H). In contrast, both EV groups exhibited higher penetration into inner ear and uptake by both outer hair cells (OHCs) and inner hair cells (IHCs) (Figure 2 I and J). Thus, the results strongly support the feasibility of μDES transfected CRISPR RNP EVs employed in gene therapy delivering to inner ear.

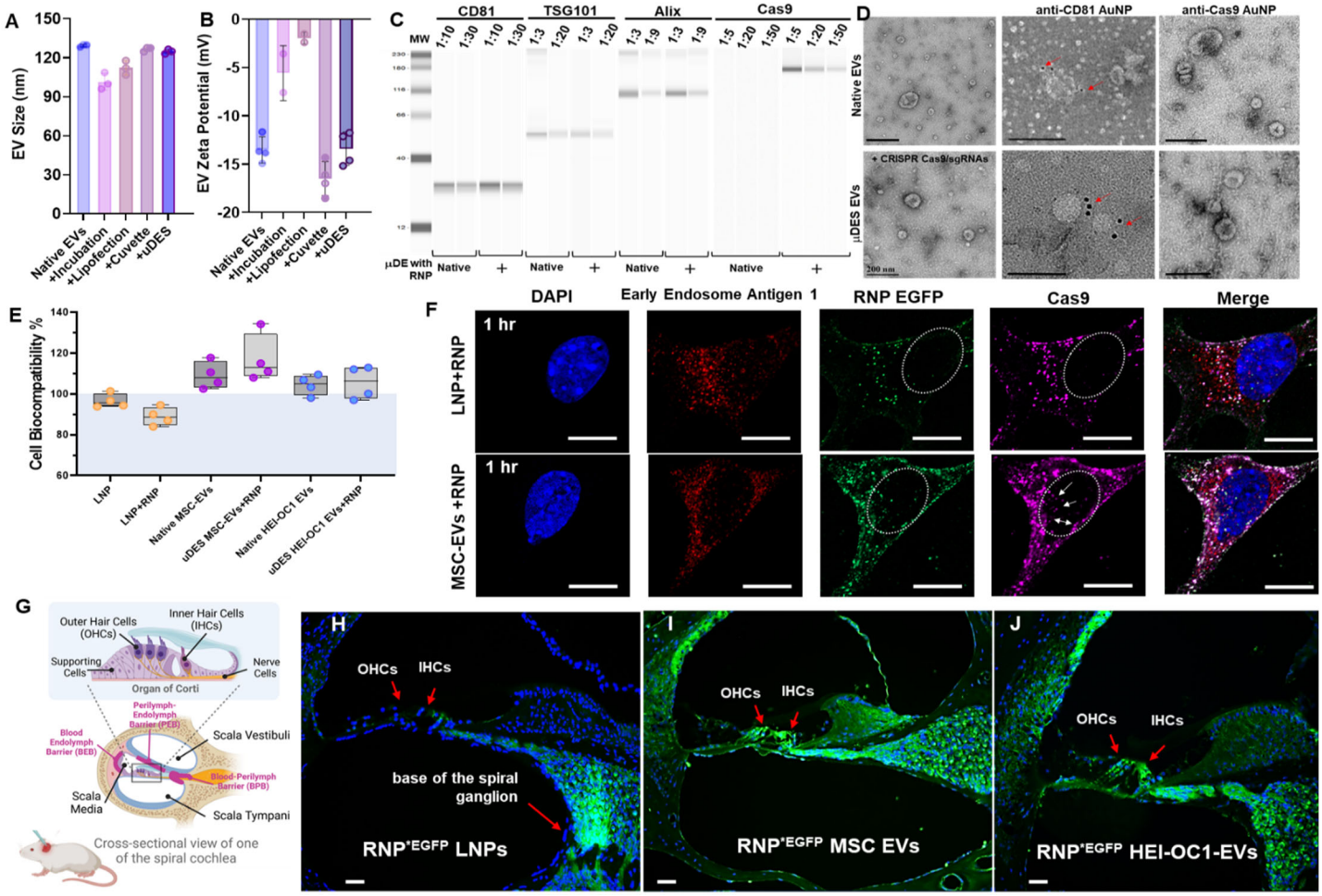

Figure 2. (A) Characterization of EV size and zeta potential **(B)** after transfection using different transfection methods with the original native EVs as the control group. **(C)** MicroWestern Blotting analysis of essential protein contents (CD81, TSG101, Alix, Cas9) derived from μDES produced RNP MSC EVs in serial dilution, with native EVs as the control group. **(D)** Immune gold nanoparticle (AuNP) staining TEM imaging analysis of μDES produced RNP MSC EVs with native EVs as the control group, in terms of CD81 surface marker expression and Cas9 surface identification. Scale bar is 200 nm. **(E)** Cell biocompatibility analysis using MTT assay with HEI-OC1 ear hair cells (~10^6) dosed with LNP group (LNP-102, Cayman Chemical, w/o RNP), MSC-EV group (w/o RNP), and HEI-OC1 EV group (w/o RNP) in ~10^9 particles. **(F)** Confocal imaging analysis of HEI-OC1 hair cell one-hour uptake dosed with RNP*^{EGFP} LNP (LNP-102, Cayman Chemical) and RNP*^{EGFP} MSC-EV group in ~10^9 particles. The white arrow indicates the cytoplasmic release and gradual entry into the nucleus. Scale bar is 10 μm. **(G)** schematic illustration of the biological barriers in the structure of Corti and cochlea including blood endolymph barrier (**BEB**), perilymph endolymph barrier (**PEB**), and blood perilymph barrier (**BPB**). Confocal tissue imaging analysis of biodistribution in the organ of Corti via posterior semicircular canal injection of **(H)** RNP*^{EGFP} LNP, **(I)** μDES produced RNP*^{EGFP} MSC EVs and **(J)** RNP*^{EGFP} HEI-OC1 EVs into Shaker-1 mice ears individually. Scale bar is 30 μm. All graphs show the mean ± SEM and biological replicates.

CRISPR design system for allele-specific editing of pathologic *Myo7a*^{sh1}

The Shaker-1 mouse model has been widely used for auditory research encoded by the deafness gene *Myo7a*, which is expressed very early in sensory hair cell development in the inner ear[45]. The *Myo7a* mutation makes up 4.5% of cases of sensorineural hearing loss evaluated in a large human patient cohort[46], which presents significant clinical populations with a high level of burden that is not addressable by current therapeutic interventions. Timely removal of mutant *myo7a* allele could potentially prevent progression of hearing loss. Therefore, we demonstrated

an allele-specific editing system using CRISPR/Cas9 with designed gRNAs targeting G-C mutations in hearing loss Shaker-1 mouse model. For in vitro validation using ear fibroblast cells from *Myo7a*$^{sh1/WT}$ mice, we screened SpCas9 and two different gRNA sets harboring *sh1* mutation modified with 2'-O-Methyl and 3'-phosphorothionate bonds on the last bases on 5' and 3' end (Figure 3A). In each gRNA set, we designed full-length and truncated forms targeting *Myo7a*^{sh1} (supplementary Table 1). The gel electrophoretic analysis shows that CRISPR/Cas9 complexes efficiently cleaved targeted *Myo7a* amplicons (supplementary Figure 3). The T7 endonuclease assay was used to screen the allele-specific editing *in vitro* in *Myo7A*$^{WT/WT}$, *Myo7A*$^{sh1/WT}$ and *Myo7A*$^{sh1/sh1}$. The indel percentage is reduced to ~25% in *Myo7A*$^{sh1/WT}$ when compared to ~45% indel percentage in *Myo7A*$^{sh1/sh1}$(supplementary Figure 4*)*. The similar halving reduction in indel percentage is also observed in other gRNA designs when targeting *Myo7a*$^{sh1/WT}$. The data supports a robust editing selectivity when targeting *Myo7A*$^{sh1/sh1}$ and *Myo7A*$^{sh1/WT}$ *in vitro*. Sanger and next generation sequencing was further used to confirm the allelic cleavage specificity and editing efficiency. ICE (Inference of CRISPR Edits, DeskTop Genetics) analysis of sanger sequencing data showed that a good amount of indel occurred only in *Myo7a*$^{sh1/WT}$, but not in *Myo7A*$^{WT/WT}$(supplementary Figure 4). The sequence percentage analyzed by CRISPResso2[47] showed that gRNA-1 and gRNA-2 have higher cleaving activity than their truncated versions respectively (Figure 3B). The indel profile revealed that the majority of CRISPR-induced variants were deletions for gRNA-1 while insertions for gRNA-2 (Figure 3C). The sequencing variations demonstrated that 94.83% of *Myo7a*^{WT} is unedited in *Myo7a*$^{sh1/WT}$. The small amount of substitution in 0.33% is possibly from PCR and sequencing background errors. In contrast, *Myo7a*^{sh1} sequences is greatly reduced to ~18% and the edited sequences account for the rest 82% in *Myo7a*^{sh1} allele. We then quantified the targeting specificity of gRNA designs by sorting out mutation pattern 5'-CCG-3' and wild type pattern 5'- CGG-3' separately when targeting *Myo7a*$^{sh1/WT}$ *in vitro*. By designing PAM sequence of gRNAs which have closer proximity to the Myo7a mutation, 95% specificity was achieved for *in vitro* editing (Figure 3D) and the wild-type allele is mostly intact after the CRISPR/Cas9 editing. Taken together, full-length of gRNA-1 and gRNA-2 have the best allele specific editing property *in vitro* thereby suggesting the potential for further *in vivo* test. Based on the global analysis of all the sequences in CRISPResso2 (Figure 3F and supplementary Figure 4), the most common mutation type is either single base deletion or single base insertion causing a frame shift in the coding sequence of *Myo7a* protein. In summary, SpCas9-gRNA-1 and SpCas9-gRNA-2 sets were specific for the *Myo7a*^{sh1} allele and robust in interfering the shaker-1 mutation at DNA level, indicating the promise for *in vivo* investigation.

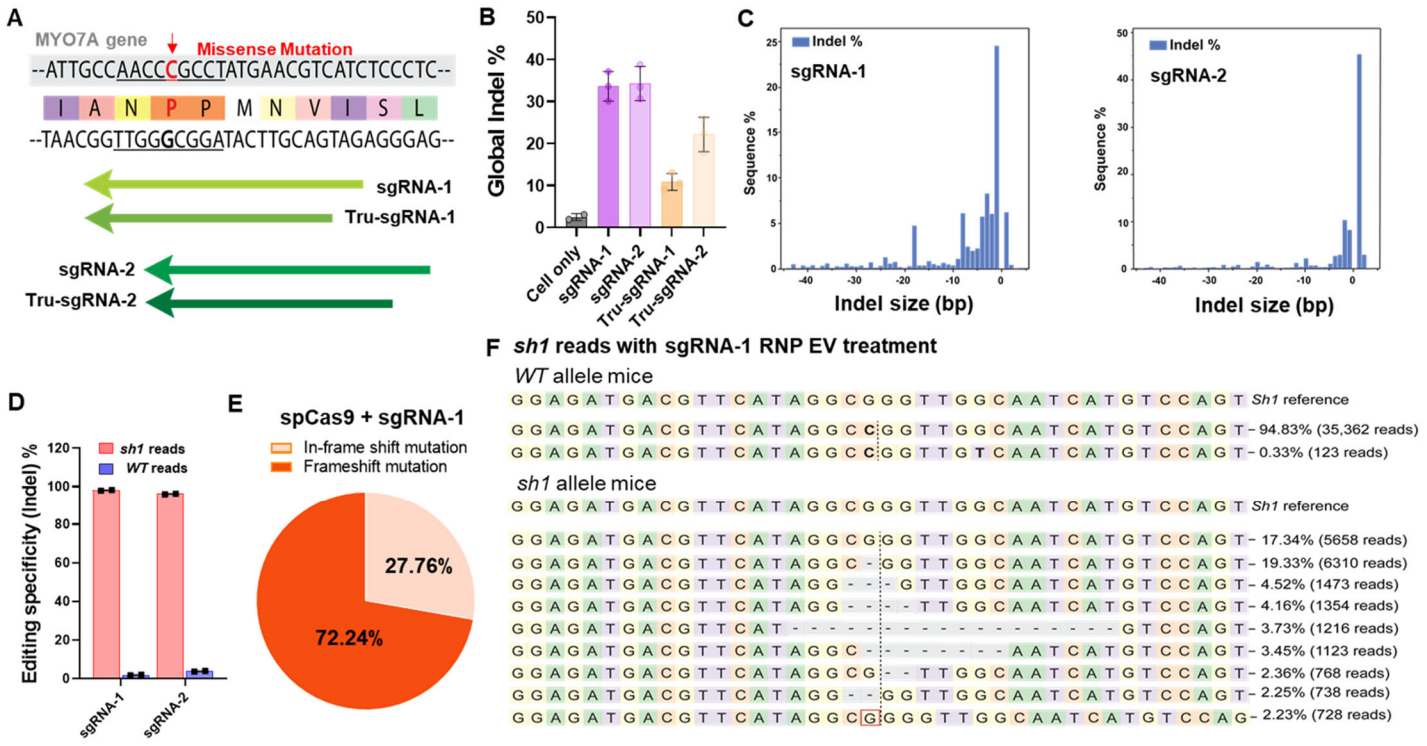

Figure 3. Design and characterization of CRISPR/Cas9 targeting Shaker-1 mutation. (**A**) Two different sgRNA and their truncated version were designed to target the allele harboring Shaker-1 mutation. **(B)** NGS results showed that indel% of gRNA-1 and gRNA-2 is up to 35% while the truncated version shows lower editing percentage. (**C**) Distribution of indel size revealed that gRNA-1 has more deletions (-1) while gRNA-2 has more insertion (+1). **(D)** Allele specific analysis demonstrated that gRNA-1 and gRNA-2 have higher preference to editing Shaker-1 allele. **(E)** Pie chart showed that the majority of editing events are frameshift mutation and some in-frame mutations. **(F)** Allele frequency tables demonstrated that shaker-1 allele is greatly reduced while WT allele is intact. All graphs show the mean ± SEM and individual biological replicates.

CRISPR loaded EVs for in vivo restoring the progression of the hearing loss

The Shaker-1 mouse wild type (+/+) and heterozygotes (+/-) initially both have normal hearing. However, the mutant heterozygotes (+/-) animals will gradually progress hearing loss till 6 months of age to be completely deaf, which serves as a good model for testing gene therapy in treating hearing loss *in vivo*. We found that *myo7a* point mutation could result in the excess oxidative stress in inner hair cells[48-49] compared to wild type animals due to the functional damage of hair cells, leading to develop a facile and straightforward assay for effectively evaluating hearing ability based on oxidative stress markers. As demonstrated in Figure 4, we administrated μDES produced CRISPR RNP MSC-EVs (~ 10^9 particles in ~10 μL) via the posterior semicircular canal into the ear in heterozygote (+/-) mice, with the good hearing wild type (+/+) mice and non-treated heterozygote (+/-) mice as the control groups. After monitoring at the month 3 and month 6, the Shaker-1 organ of Corti tissues were extracted for immunohistochemistry based oxidative stress analysis. The oxidative stress markers 4-Hydroxynonenal (4-HNE) and 3-Nitrotyrosine (3-NT) were stained in green fluorescence. The heterozygous (+/-) mice show high expression level of both oxidative stress markers 4-HNE and 3-NT at 3 and 6 months of age in the inner ear hair cells (Figure 4 white arrows), in contrast to normal hearing wild type (+/+) mice with no

oxidative stress marker expression. Interestingly, in our treatment group of heterozygous (+/-) mice, both 4-HNE and 3-NT expression level indicating the oxidative stress was significantly reduced to the unnoticeable level at 6 months of age, indicating the recovery of hair cell auditory function and elimination of pathogenic myosin VIIa allele.

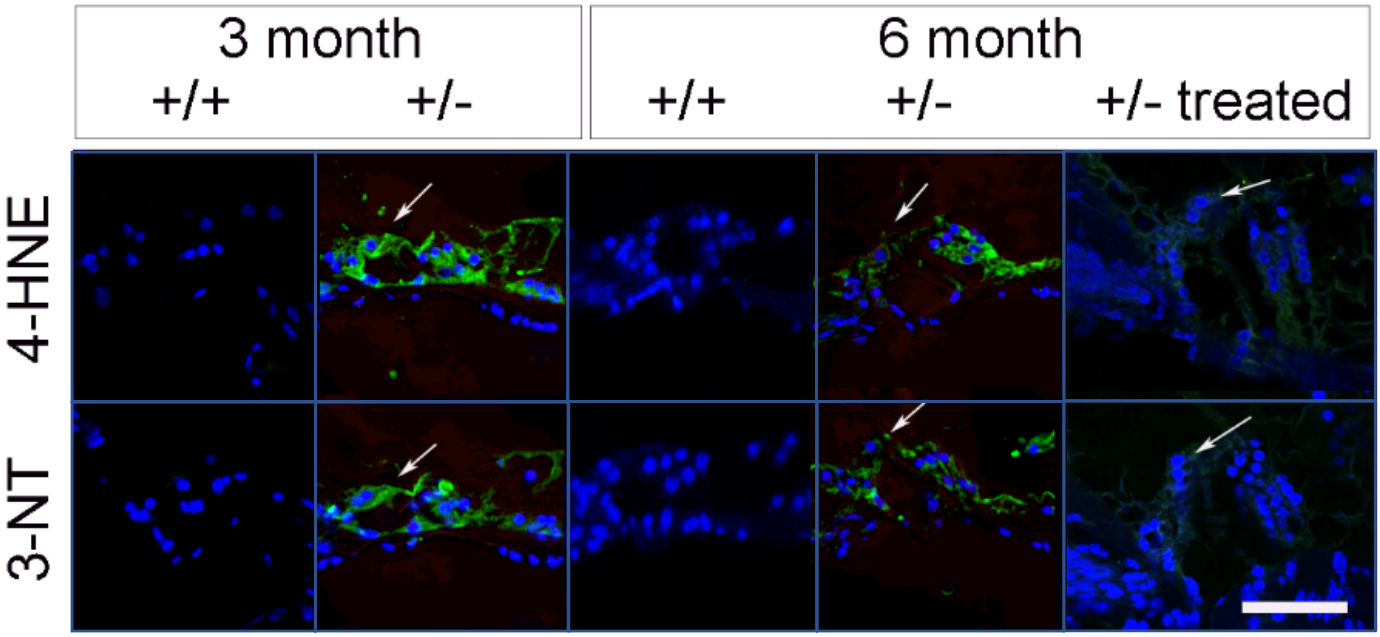

Figure 4. Immunohistochemistry for oxidative stress in the Shaker-1 organ of Corti. The inner hair cell is indicated by the white arrow. Primary staining with 4-Hydroxynonenal (4-HNE) 1:50, and 3-Nitrotyrosine (3-NT) 1:50. Secondary staining 1:1000, nuclei labelled with DAPI. +/+, wild type; +/-, heterozygous Shaker 1 mice. Heterozygous mice show labelling for oxidative stress markers at 3 and 6 months of age whereas wild type mice show no labelling. Heterozygous mice treated with Crispr-EVs that eliminate the pathogenic myosin VIIa allele show no evidence of oxidative stress at 6 months of age, indicating the recovery of inner hair cell auditory function. Scale bar is 150μm.

To further evaluate the gene editing efficiency at molecular precision *in vivo* using our μDES produced CRISPR RNP MSC-EVs, we administrated EVs (~ 10^9 particles in ~10 μL) via the posterior semicircular canal into the left ear with right ear as the untreated control group in Shaker-1 heterozygotes (Figure 5A). The tissue of Corti was extracted in week 4 after injection for mRNA sequencing (Figure 5B-C). The heterozygous Shaker 1 mutant/wild type mice hearing ability after the treatment of RNP-EVs was followed over six months of age (Figure 5D-F) based on the hearing threshold results from ABR test. In first 4 weeks of treatment, the μDES produced CRISPR EVs group already exhibited the gene changes at the mRNA level, which showed improved gene editing ability compared with RNP-LNPs and cuvette transfected RNP-EVs (Figure 5B). Such gene editing performance differences could potentially be due to the ability and efficiency of delivery carriers entering into the hair cells. The editing efficiency was amplified at mRNA level given the fact that mRNA of *Myo7a* was only transcribed in hair cells, although *myo7a* gene exists in every cell type in the organ of Corti.

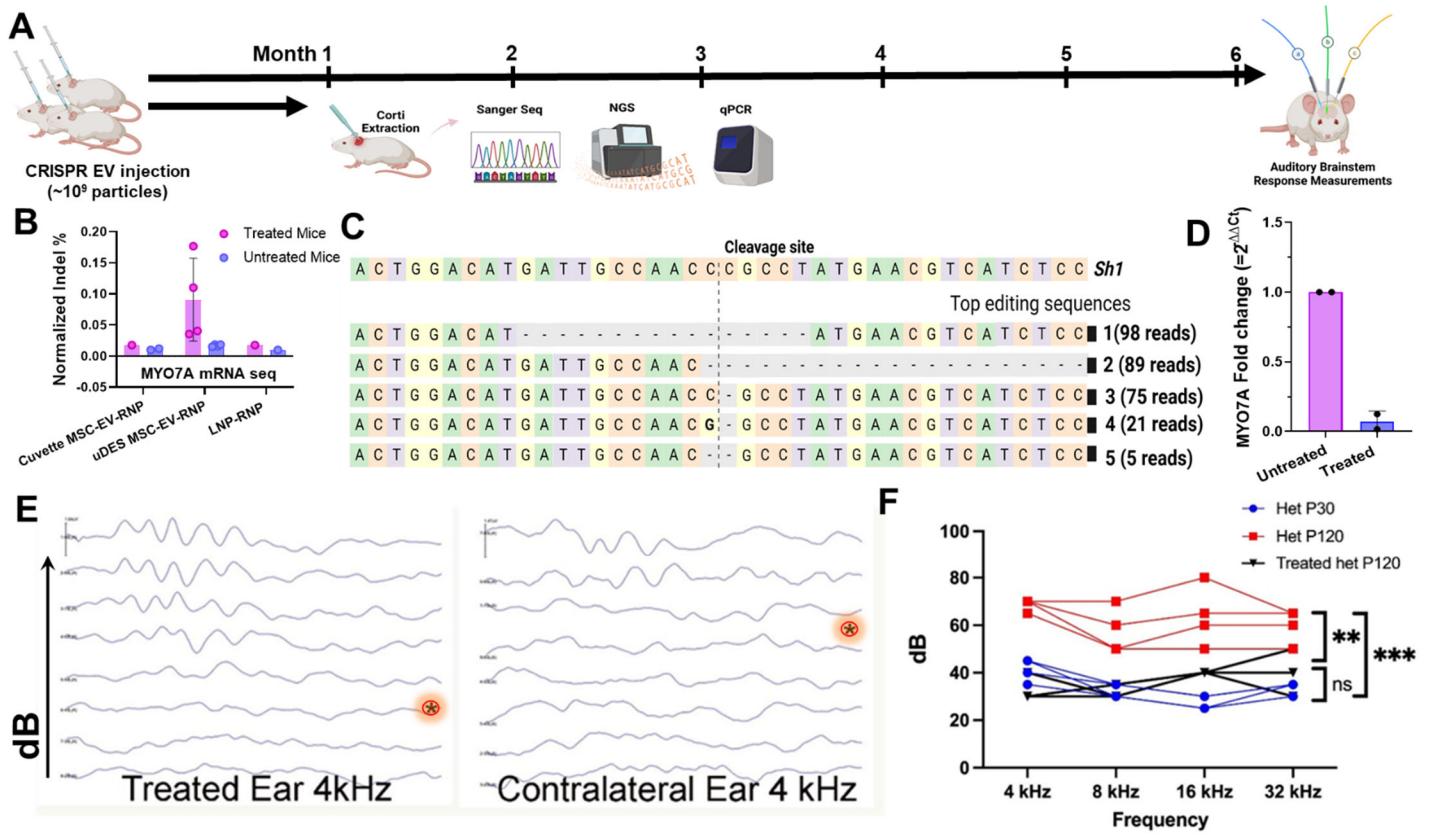

Figure 5. (A) Schematic illustration of animal testing schedule. **(B)** The indel% mRNA sequencing analysis of *Myo7a* sequence changes from extracted Corti tissue from Shaker 1 heterozygotes mice in week 4 after CRISPR EV injection, with RNP-LNPs and Cuvette transfection method as control groups. **(C)** Distribution of resulted sequences treated by µDES produced CRISPR MSC EVs in week 4 from mRNA sequencing analysis. The most common edited sequences were shown. **(D)** qPCR analysis of *Myo7a* fold change from extracted Corti tissue in month 6 after injection of mDES produced CRISPR MSC EVs, which showed significant reduction of mutant *Myo7a* in treatment group. **(E)** Representative auditory brainstem responses (ABRs) recorded from shaker-1 heterozygotes mice left ear treated with µDES produced CRISPR MSC EVs in month 6, and right ear without treatment. The start showed the hearing ability baseline **(F)** The groups of shaker-1 heterozygotes mice in p30 as the normal hearing control group, and p120 developing severe hearing loss, to compare with p120 group treated with µDES produced CRISPR MSC EVs, which indicates positive therapeutic function for preventing progression of hearing loss.

At 6 months, the pathogenic myosin VII a allele was nearly removed (Figure 5D). These mice at P30 have normal hearing serving as the control group in Figure 5F blue line, and later on developed a severe sensorineural hearing loss by six months of age in Figure 5F red line Het P120. In contrast, the treated p120 group of mice displayed significant restoration of hearing ability (black line) compared to untreated p120 group of mice (red line). There is no significant difference from treated p120 group of mice (Black) with p30 normal hearing group of mice (Blue), indicating that our developed CRISPR EVs can remove pathogenic myosin VII a allele in these heterozygous mice for restoring hearing ability.

DISCUSSION

The development of gene therapy correcting or eradicating genetic mutations for restoring functional protein expression is essential in maintaining sensory mechanotransduction and regenerating cochlear hair cells, thereby, to improve hearing function[8]. It not only requires highly targeted gene editing complexed, but also most effective and cell-specific delivery platforms. Presently, more challenges with the application of viral vectors or lipid nanoparticles were found to deliver functional genetic materials into auditory sensory system, due to the low tolerance from sensitive hair cells to toxicity and the intrinsic anatomical barriers. The safety of the treatment is concerned with the transgene and constitutive expression of gene editing complexes from eukaryotic organelles, as well as the ototoxicity from chemical compounds, for future clinical translation. Using EVs to encapsulate CRISPR/Cas9 gene editing agents provides a transient way to target auditory hair cells for achieving permanent genetic alteration on the deafness gene such as shaker-1 allele. Such treatment prevents supplementary treatment to attenuate the potential ototoxicity induced by delivery vehicles or overexpression of CRISPR/Cas9 complexes *in vivo*. More importantly, EVs exhibited excellent tissue penetration ability to specifically access and target inner hair cells as we observed in our shaker-1 mouse model (Figure 2).

Droplet-based electro-transfection has been reported to have higher mass and heat transfer demonstrated in single cell electroporation. EVs derived from donor cells also consist of lipid bilayer and similar membrane proteins composition on cells. However, nanosized EVs contain more compact membrane curvatures and strong brownie motion. Using microfluidic droplet-based electroporation to maximize the encapsulation of cargos into EVs, in turn, maximize the gene editing efficiency in vitro and in vivo, has been demonstrated with approximately 10-fold increase on the loading amount of CRISPR/Cas9 RNP into EVs. The throughput is hundred-fold increase compared with conventional cuvette electro-transfection method. Fast continuous flow through with droplet also prevents direct contact of EVs with electrodes for retaining EV natural integrity and stability. Such platform offers an easily amenable approach for scaling up by integrating multiple chip units for future GMP grade manufacturing of cargo-loaded EVs. The rapid loading of CRISPR RNP into EVs will allow the delivery of Cas9 without using a split vector approach, which enables customization of sgRNAs for addressing different mutant alleles within one gene, thus, opening a new avenue for personalized precision gene therapy via tailoring patient genetic heterogeneous mutation background.

MATERIALS AND METHODS

Materials and reagents

All chemical reagents and materials were purchased from ThermoFisher unless otherwise specified. Modified gRNAs were synthesized and quantified by Synthego. NLS-*sp*Cas9-NLS, EGFP-*sp*Cas9-NLS nucleases, anti-Cas9 antibody (Clone 4A1) were purchased from Genscript. All of DNA oligos were purchased from Integrated DNA Technologies. The collagenase IV was obtained from STEMCELL Technologies. SYLGARD™ 184 Silicone Elastomer Kit was purchased from Dow Silicones Corp. Master Mold for PDMS device was obtained from CADworks3D. Q5 high-fidelity DNA polymerase was purchased from New England Biolabs. Human bone

marrow-derived conditioned culture medium and human umbilical cord-derived conditioned culture medium for extracellular extraction were purchased from EriVan Bio. SM-102 LNP in ethanol was the generous gift from Dr. Fan Zhang, in the College of Pharmacy at the University of Florida. 6nm Goat anti-Mouse and anti-Rabbit, IgG, Immuno Gold reagents were purchased from AURION.

Droplet generator on chip

The 3D structure of microfluidic device was designed and drawn by SOLIDWORK CAD. The resin mold for PDMS casting containing 200 µm flow and 500 µm electrode channels, 150 µm as nozzle for droplet generation, was printed by µMicrofluidics Printer (CADworks3D, 30 µm resolution). Briefly, CAD files was opened by utility.exe that is connected to µMicrofluidics Printer. The software setting for printing as follows: 50 µm as thickness, 0.1 for grid size, 40% Power ratio. The microstructure was then sliced and ready to be launched for printing. The resulting resin mold was then soaked in 100% Ethanol or isopropanol for 10 min to remove the free resin before the final UV curing step. And then the resin mold was dried with compressed Nitrogen. The soaking-drying cycles have to be repeated several times until there is no shiny free resin on the microstructure. Each side of resin mold was then cured in the Creative Cure Zone (CADworks3D) for another 10min twice for further photopolymerization and solidification of microstructures. The resin mold was then ready for PDMS casting. PDMS was prepared using the standard 10 : 1 (base to curing agent) ratio. The PDMS mixture was stirred completely at least 3 min and then degassed for at least 30 min before being poured into the 3D-printed molds and then baked at 75°C for 3 hours. After the surface activation of molded PDMS pieces using a corona discharger and the microscope plate, PDMS molds were then assembled and bound onto the microscopic plate as the droplet-based electro-transfection device.

Electrodes with L shape were tailored to fit into electroporation chambers designed in µDES and then manually inserted into the electroporation sites to align well with each other. The 1/16 OD, 1/32 ID tubings were then inserted into the inlets and outlets in µDES. To avoid any potential pressure leakage that can result in the unstable flow rate in µDES, the additional PDMS was then added to the area surrounding the inlets, outlets and electroporation sites before use. And then the device was baked in the oven at 75°C for 30min. The resulting µDES is ready to the following electroporation.

COMSOL Simulation

The proposed microfluidic device was fine-tuned using the COMSOL Multiphysics software package. The device's mathematical model involves fluid flow and electromagnetism. For both models a standard linear triangular extra-fine mesh was assigned to the geometry. To observe the geometric evolution of our droplets, we used the computational fluid dynamics system (CFD) module using the laminar two-phase flow. For this simulation, the oil phase material was defined as FC-40 with a density of 1850 kg/m^3 and a dynamic viscosity of 0.0018 Pa/s. Microfluidic flows are defined by the Navier Stokes equation where ρ is the density of the fluid, u is the velocity of the field, t is time and P is the pressure field:

$$\rho\left(\frac{\delta u}{\delta t} + u \cdot \nabla u\right) = \nabla P + \mu \nabla^2 + f$$

The physics of the electroporation system of the device were defined using the AC/DC module to simulate the electric field distribution in the microfluidics electroporation model. The material of the droplet was defined as electrolytic buffer with a conductivity of 1x10^{-4} S.m^{-1}. The electrical conductivity of the electrode was defined by the composition of the Platinum-iridium wire as 9.43x10^6 S.m^{-1}. In steady conditions, the flow of electric currents within a conducting fluid follows Ohm's law:

$$J = \sigma E + J_e$$

Here, J represents the total current density within the material while σ represents the electrical conductivity measured in S.m^{-1}. E is the electrical field strength measured in V.m^{-1} and J_e represents the current density.
Moreover, to mathematically describe the electric field that acts upon the droplet within the microfluidic device, we use the induced potential difference $\Delta\Psi_i$ at a point M of the droplet membrane at any time t

$$\Delta\Psi_i(M,t) = fg(\lambda)Er\cos(\theta)\left(1 - e^{\frac{-t}{\tau_c}}\right)$$ [50]

The results of this simulation were then used to adjust and optimize the device's design for the intended application. Overall, the use of the COMSOL Multiphysics software package allowed for a detailed and accurate analysis of the proposed microfluidic device, ensuring its optimal performance.

Electro-transfection of CRISPR into Extracellular Vesicles

Neon electro-transfection system

EVs in 1x PBS buffer were firstly transferred into Neon R buffer by using 30 kDa cutoff ultrafiltration column to reach the final concentration of 10^{10} EVs/mL. Basically, EVs were added into the pre-washed 30K cutoff column and centrifuge at 7000 xg for 8 min and then resuspend the concentrated EV (~80 µL) in 400µL Neon R buffer to centrifuge again under the same condition. The resulting EVs in Neon R buffer (~60µL) was placed on ice immediately for later use. To electro-transfect CRISPR/Cas9 complexes into EVs, gRNAs and EGFP-Cas9 nuclease were firstly pre-mixed together in 45µL Neon R buffer and self-assembled at room temperature for 10min and then added into EVs solution to obtain 6µM of EGFP-Cas9 and 9µM of gRNA in the ready-to-electro-transfection solution (~106µL). To stabilize the membrane, 1250mM trehalose was prepared in PBS buffer without Ca^{2+} and Mg^{2+} and then 4.4µL added to the ready-to-electro-transfection solution to have 50mM trehalose in the final solution. The addition of trehalose increased the viscosity of electro-transfection solution therefore, to maintain the viscosity balance in Neon electroporation system, 120µL of 1250mM trehalose was added to per 3mL Neon electrolytic buffer. 1500V, 20ms, 1 pulse was used to electro-transfect CRISPR/Cas9 complexes into HEI-OC1 derived EVs with 100uL Neon platform. The resulting electro-transfected CrisprEV was gently transferred to 1.5mL protein low binding Eppendorf tube for membrane recovery at room temperature for 10min. And then 500uL PBS buffer at room temperature was added to EV solutions followed by the further membrane recovery at 37°C for 20 min. The resulting CrisprEV was stored in -20°C for the downstream purification and analysis.

High-throughput droplet-based µDES

Water-in-oil droplets were generated at the flow-focusing junction inside the µDES. As described previously, EVs were first transferred to Cytoporation® Media T (BTXpress™, USA) and then mixed with 5µM gRNA-Cas9 RNP (gRNA:Cas9 molar ratio=1.5:1) at the concentration of EVs 10^{10}/mL. The resulting mixture was delivered into the device as the dispersed aqueous phase. The oil phase contained FC-40 mixed with 2 weight % 008-FluoroSurfactant (RAN Biotech). A microfluidic pressure flow controller (PreciGenome) was used to generate the droplets with the diameter of around 1000µm at 3.0-3.8µL/min of the aqueous solution and 1.5-2µL/min of the oil phase. The electroporation was performed ranging from 10-60V by using direct current-based power supply and the resulting emulsion was collected within an Eppendorf tube or the microplate analyzed under the inverted microscope (Cytation 5, BioTek).

Purification of CrisprEVs

The isolation of aqueous phase containing CrisprEVs was performed under the centrifuge at 2000-3000xg for 5-10min at room temperature. The aqueous phase was then collected by the pipettes and transferred to a new Eppendorf tube for the downstream purification. To remove excessive His tagged CRISPR/Cas9 complexes from CrisprEVs, 100µL Ni Sepharose high performance beads (GE Healthcare) were firstly washed with 10 volume of cold 1x PBS buffer and then pre-equilibrated in PBS buffer for 10min. The beads were then incubated with per 100µL CrisprEV at 4°C for 0.5-1 hours on the rocker. The unbound CrisprEV was then collected in 1 mL of cold 1x PBS buffer while the excessive CRISPR/Cas9 bound on the column. The purified CrisprEV was then concentrated with 30 kDa ultrafiltration column under the same condition mentioned above and stored in -80°C for further analysis.

Characterization of CrisprEV

Nanoparticle tracking analysis

The size and particle number of purified EV and CrisprEV were analyzed by nanoparticle tracking analysis (NTA) using the NanoSight NS300 instrument (Malvern Instruments, UK) supplied with a blue laser (488 nm). Briefly, 25 µL of the final EV solutions was diluted in 1:20 for NTA analysis. A solution of 400 µL was injected into the sample chamber and each trajectory measurement of every sample was repeated five times. Data analysis was performed in NTA 3.4 software (NanoSight) with the following software settings for capture and analysis: camera level=16, screen gain=1, detection threshold=18.

Surface Charge

The zeta potential of the resulting EVs was measured by dynamic laser scattering (Litesizer 500, Anton Paar). Briefly, 25 µL of the final EV solutions diluted in 1:20 with 10% PBS buffer was injected into disposable folding capillary cuvette and each zeta potential measurement was conducted five times. The final measurement is conducted with 2min for pre-equilibrium, under room temperature by selecting PBS as the referenced conductivity.

Loading efficiency of Cas9 protein

The concentration of CRISPR/EGFP-Cas9 loaded into EVs was measured by Cytation5 (BioTek). Firstly, the standard curve of fluorescent intensity of EGFP-Cas9 in PBS buffer was obtained from Cytation 5 with a serial dilution of EGFP-Cas9 in the 96 well microplate. Each dilution was conducted and measured in duplicates. 35uL of the final EV was diluted in 1:1 with PBS buffer and then added to the microplate above and the fluorescent intensity of the resulting solution measured under the same condition with the standard curve. To further quantify the loading efficiency of CRISPR/EGFP-Cas9 in single EV, 25uL of the final EV solutions diluted in 1:40 with PBS buffer was then injected into ZetaView NTA (ParticleMetrix, Germany) for the quantification of $EGFP^+$ EV. Basically, the diluted EVs were measured in scattering and fluorescent mode by using particle number/sensitivity measurement in fluorescent NTA (fNTA) with laser 488nm. By using reference polystyrene beads with Ex 488nm, the sensitivity scale was set at 96-98 with 100% fluorescent labeled beads. And then the final percentage of $EGFP^+$ EVs was normalized against that of the reference beads under the same sensitivity in the fluorescent mode.

Loading efficiency of gRNA

The resulting CrisprEVs were first incubated with 1U of proteinase K followed with 1X Halt™ proteinase inhibitor cocktail (Thermo, USA). The solutions were then incubated with 1U RNase A (Thermo, USA) following the manufacture's protocol. The resulting RNP-EVs were then directly employed to extract total RNA by using Qiagen kit. The final RNA concentration for RT-qPCR was quantified with Quant-it™ RiboGreen RNA assay kit. For RT-qPCR, 1ng of total RNA was used for 20µL of AMV reverse transcriptase at 55°C for 1 hour following the manufacture's procedure (NEB, USA). The final cDNA was aliquoted to 4 individual qPCR reactions by using the primers in **Table S1**.

Automated western blotting of CrisprEVs

Total protein extracts from purified CrisprEVs were prepared in the one volume of lysis solution, RIPA buffer (Thermo), followed by 5min sonication, 30s vortex. Protein concentration was then determined by the Micro BCA Protein Assay (Thermo, USA). Protein extracts (100-150ng per lane) were added and separated in the cartridge compatible with Wes Instrument (Bio-Techne, USA). Simple Western was performed and imaged according to the manufacture's procedure.

Indel Analysis

T7E1 assay

200 ng purified amplicons were denatured and re-annealed by following the manual of GeneArt Cleavage detection kit. The re-annealed amplicons were then incubated with T7 endonuclease I for 30min at 37°C. The final solution was then immediately added to the well of 0.8-2% SYBR safe prestained E-gel and run for 26 min in the E-gel running system (Thermo, USA). The gel was then imaged with Typhoon imager using the Cy2 channel. The band intensity was quantified with ImageQuant and Indel % was obtained by using equation: $(1- (1-\text{fraction cleaved})^{1/2})$.

Sanger sequencing and TIDE analysis

Purified amplicons with more than 200 nt flanking sequences were quantified with Cytation 5 and then diluted to the final concentration at 5 ng/µL. The resulting amplicons together with reverse primer (5'-GCGTAGGAGTTGGACTTGATAG -3') were then submitted to Sanger sequencing provided by Genewiz. The sequencing data were opened with UGENE software for imaging and visualization of amino acid sequences. The DNA sequencing data were then uploaded to *TIDE*, the online quantitative tool of Indel analysis of sequencing trace of CRISPR editing. The Indel % was obtained by comparing the decomposition frequency of CRISPR treated groups to the one without the treatment of CRISPR. The same gRNAs were entered into *TIDE* for both full length of gRNAs and the corresponding truncated counterparts due to the same cutting site.

CRISPResso bioinformatic analysis

The sequences of amplicons with primer pairs, *Myo7a*_FP_NGS and *Myo7a*_RP_NGS were obtained from Amplicon-EZ in Genewiz. The Indel analysis and mutation types were identified with online CRISPR bioinformatic tool, *CRISPResso2*, with Exon sequences: 5'-CCTTGGGGAACTTGCTCTCCTCATCGATGAGGGAGATGACGTTCATAGGCGGGTTGGCAATCATGTCCAGTGCTTCCTGGTTGTCAGTGAACTCAATGTGCAGCCAGTCGATGCTCTCCAGGTCGTACTCCTC -3'. The sequences of gRNAs and the associated truncated counterparts were used in the *CRISPResso2* analysis.

Immunohistochemical and histology

The animals were anesthetized with phenobarbital (585 mg/kg) and phenytoin sodium (75 mg/kg) (Beuthanasia®-D Special, Schering-Plough Animal Health Corp., Union, NJ, Canada) i.p. and sacrificed via intracardiac perfusion with 4% paraformaldehyde in phosphate buffered saline (PBS). The temporal bones were removed, the stapes extracted, and the round window was opened. The temporal bones were postfixed overnight in 4% paraformaldehyde in PBS at 4°C. After rinsing in PBS three times for 30 min, the temporal bones were decalcified in 10% EDTA (ethylene diamine tetraacetic acid) for 48h. The temporal bones were rinsed in PBS and embedded in paraffin. Seven µm sections were cut in parallel to the modiolus, mounted on Fisherbrand® Superfrost®/Plus Microscope Slides (Fisher Scientific, Pittsburgh, PA, U.S.A.) and dried overnight. Samples were deparaffinized and rehydrated in PBS two times for 5 min, then three times in 0.2 % Triton X-100 in PBS for 5 min and finally in blocking solution 0.2 % Triton X-100 in PBS with 10 % fetal bovine serum for 30 min at room temperature. After blocking, specimens were treated with anti-myosin VIIa rabbit polyclonal antibody (Proteus® BioSciences, Inc., Ramona, Calif., USA) diluted 1:100 in blocking solution. The tissue was incubated for 48h at 4 ˚C in a humid chamber. After three rinses in 0.2 % Triton X-100 in PBS, immunofluorescent detection was carried out with anti-rabbit IgG (1:50; Alexa Fluor 488 nm; Invitrogen®Inc.). The secondary antibody was incubated for 6h at room temperature in a humid chamber. The slides were rinsed in 0.2 % Triton X-100 in PBS three times for 5 min and finally coverslipped with ProLong® Gold antifade reagent (Invitrogen™ Molecular Probes, Eugene, OR, U.S.A.).

Inner ear tissue dissection for HTS

Both sides of organ of Corti was collected after 6 months since the intratympanic administration of CrisprEVs on the left side while untreated on the right side. DNA and RNA samples were collected by following the manufacturer's instruction of QIAgen MagAttract HMW DNA Kit and miRNAeasy Mini Kit with DNAse treatment respectively. The resulting nucleic acid samples were then quantified with Agilent Genomic DNA Tape assay and RNA Screen Tape assay respectively. Genomic DNA was then amplified with the primer sets (IDT, USA) for sequencing with 2 x 250 Miseq, nanoflow cell with 1 million (0.5Gbp), FP_Myo7a_HTS, 5'- **TCGTCGGCAGCGTCAGATGTGTATAAGAGACAG**CCCAGGTCAAGCCAATTCTAT-3'; and RP_Myo7a_HTS, 5'- **GTCTCGTGGGCTCGGAGATGTGTATAAGAGACAG**CTTCGAGCAGCTCTGCATTA -3'. cDNA library of mRNA and full transcripts were prepared by using the amplicons for mRNA of Myo7a shown in the **Table S1**.

Statistical Analysis

Statistical analyses were performed using GraphPad Prism 9.0.0 for Microsoft. Data were presented as biological replicates and were shown as means±SD or range as indicated in the corresponding figure legends. Meanwhile, sample sizes and the statistical tests used were described in detail in the corresponding figure legends. Unpaired Student's t test and one/two-way analysis of variance (ANOVA) tests were performed following the appropriate post hoc test when more than two groups were compared. For all analyses, $P<0.05$ was assigned as statistically significant.

List of Supplementary Materials

Present a list of the Supplementary Materials in the following format.

Fig S1 to S6 for multiple supplementary figures

Tables S1 to S2 for multiple supplementary tables

REFERENCES:

1. Muller, U.; Barr-Gillespie, P. G., New treatment options for hearing loss. *Nat Rev Drug Discov* **2015,** *14* (5), 346-65.
2. Foster, A. C.; Jacques, B. E.; Piu, F., Hearing loss: The final frontier of pharmacology. *Pharmacol Res Perspect* **2022,** *10* (3), e00970.
3. Tao, Y.; Lamas, V.; Du, W.; Zhu, W.; Li, Y.; Whittaker, M. N.; Zuris, J. A.; Thompson, D. B.; Rameshbabu, A. P.; Shu, Y.; Gao, X.; Hu, J. H.; Pei, C.; Kong, W. J.; Liu, X.; Wu, H.; Kleinstiver, B. P.; Liu, D. R.; Chen, Z. Y., Treatment of monogenic and digenic dominant genetic hearing loss by CRISPR-Cas9 ribonucleoprotein delivery in vivo. *Nat Commun* **2023,** *14* (1), 4928.
4. Li, L.; Chao, T.; Brant, J.; O'Malley, B., Jr.; Tsourkas, A.; Li, D., Advances in nano-based inner ear delivery systems for the treatment of sensorineural hearing loss. *Adv Drug Deliv Rev* **2017,** *108*, 2-12.
5. Shubina-Oleinik, O.; Nist-Lund, C.; French, C.; Rockowitz, S.; Shearer, A. E.; Holt, J. R., Dual-vector gene therapy restores cochlear amplification and auditory sensitivity in a mouse model of DFNB16 hearing loss. *Sci Adv* **2021,** *7* (51), eabi7629.
6. Michael, M.; Juliane, W. S.; Axel, R.; Christian, L.; Athanasia, W.; Hinrich, S.; Anke, L.-S.; Brigitte, S.; Hildegard, B.; Bernd, A.; Axel, S., Gene therapy as a possible option to treat hereditary hearing loss. *Medizinische Genetik* **2020,** *32* (2), 149--159.
7. Gyorgy, B.; Nist-Lund, C.; Pan, B.; Asai, Y.; Karavitaki, K. D.; Kleinstiver, B. P.; Garcia, S. P.; Zaborowski, M. P.; Solanes, P.; Spataro, S.; Schneider, B. L.; Joung, J. K.; Geleoc, G. S. G.; Holt, J. R.; Corey, D. P., Allele-specific gene editing prevents deafness in a model of dominant progressive hearing loss. *Nat Med* **2019,** *25* (7), 1123-1130.
8. Li, S.; Mecca, A.; Kim, J.; Caprara, G. A.; Wagner, E. L.; Du, T. T.; Petrov, L.; Xu, W.; Cui, R.; Rebustini, I. T.; Kachar, B.; Peng, A. W.; Shin, J. B., Myosin-VIIa is expressed in multiple isoforms and essential for tensioning the hair cell mechanotransduction complex. *Nat Commun* **2020,** *11* (1), 2066.
9. Delmaghani, S.; El-Amraoui, A., Inner Ear Gene Therapies Take Off: Current Promises and Future Challenges. *J Clin Med* **2020,** *9* (7).
10. Warnecke, A.; Harre, J.; Staecker, H.; Prenzler, N.; Strunk, D.; Couillard-Despres, S.; Romanelli, P.; Hollerweger, J.; Lassacher, T.; Auer, D.; Pachler, K.; Wietzorrek, G.; Kohl, U.; Lenarz, T.; Schallmoser, K.; Laner-Plamberger, S.; Falk, C. S.; Rohde, E.; Gimona, M., Extracellular vesicles from human multipotent stromal cells protect against hearing loss after noise trauma in vivo. *Clin Transl Med* **2020,** *10* (8), e262.
11. Joshi, B. S.; Ortiz, D.; Zuhorn, I. S., Converting extracellular vesicles into nanomedicine: loading and unloading of cargo. *Materials Today Nano* **2021,** *16*, 100148.
12. Gyorgy, B.; Sage, C.; Indzhykulian, A. A.; Scheffer, D. I.; Brisson, A. R.; Tan, S.; Wu, X.; Volak, A.; Mu, D.; Tamvakologos, P. I.; Li, Y.; Fitzpatrick, Z.; Ericsson, M.; Breakefield, X. O.; Corey, D. P.; Maguire, C. A., Rescue of Hearing by Gene Delivery to Inner-Ear Hair Cells Using Exosome-Associated AAV. *Mol Ther* **2017,** *25* (2), 379-391.
13. Yom-Tov, N.; Guy, R.; Offen, D., Extracellular vesicles over adeno-associated viruses: Advantages and limitations as drug delivery platforms in precision medicine. *Adv Drug Deliv Rev* **2022,** *190*, 114535.
14. Wan, T.; Zhong, J.; Pan, Q.; Zhou, T.; Ping, Y.; Liu, X., Exosome-mediated delivery of Cas9 ribonucleoprotein complexes for tissue-specific gene therapy of liver diseases. *Sci Adv* **2022,** *8* (37), eabp9435.
15. Yang, Z.; Shi, J.; Xie, J.; Wang, Y.; Sun, J.; Liu, T.; Zhao, Y.; Zhao, X.; Wang, X.; Ma, Y.; Malkoc, V.; Chiang, C.; Deng, W.; Chen, Y.; Fu, Y.; Kwak, K. J.; Fan, Y.; Kang, C.; Yin, C.; Rhee, J.; Bertani, P.; Otero, J.; Lu, W.; Yun, K.; Lee, A. S.; Jiang, W.; Teng, L.; Kim, B. Y. S.; Lee, L. J., Large-scale generation of functional mRNA-encapsulating exosomes via cellular nanoporation. *Nat Biomed Eng* **2020,** *4* (1), 69-83.
16. Alvarez-Erviti, L.; Seow, Y.; Yin, H.; Betts, C.; Lakhal, S.; Wood, M. J., Delivery of siRNA to the mouse brain by systemic injection of targeted exosomes. *Nat Biotechnol* **2011,** *29* (4), 341-5.
17. Kumar, S.; Karmacharya, M.; Michael, I. J.; Choi, Y.; Kim, J.; Kim, I.; Cho, Y.-K., Programmed exosome fusion for energy generation in living cells. *Nature Catalysis* **2021,** *4* (9), 763-774.
18. Warnecke, A.; Prenzler, N.; Harre, J.; Kohl, U.; Gartner, L.; Lenarz, T.; Laner-Plamberger, S.; Wietzorrek, G.; Staecker, H.; Lassacher, T.; Hollerweger, J.; Gimona, M.; Rohde, E., First-in-human intracochlear application of human stromal cell-derived extracellular vesicles. *J Extracell Vesicles* **2021,** *10* (8), e12094.

19. Zhu, Q. F.; Heon, M.; Zhao, Z.; He, M., Microfluidic engineering of exosomes: editing cellular messages for precision therapeutics. *Lab Chip* **2018,** *18* (12), 1690-1703.
20. Cecchin, R.; Troyer, Z.; Witwer, K.; Morris, K. V., Extracellular vesicles: The next generation in gene therapy delivery. *Mol Ther* **2023,** *31* (5), 1225-1230.
21. Herrmann, I. K.; Wood, M. J. A.; Fuhrmann, G., Extracellular vesicles as a next-generation drug delivery platform. *Nat Nanotechnol* **2021,** *16* (7), 748-759.
22. You, Y.; Tian, Y.; Yang, Z.; Shi, J.; Kwak, K. J.; Tong, Y.; Estania, A. P.; Cao, J.; Hsu, W. H.; Liu, Y.; Chiang, C. L.; Schrank, B. R.; Huntoon, K.; Lee, D.; Li, Z.; Zhao, Y.; Zhang, H.; Gallup, T. D.; Ha, J.; Dong, S.; Li, X.; Wang, Y.; Lu, W. J.; Bahrani, E.; Lee, L. J.; Teng, L.; Jiang, W.; Lan, F.; Kim, B. Y. S.; Lee, A. S., Intradermally delivered mRNA-encapsulating extracellular vesicles for collagen-replacement therapy. *Nat Biomed Eng* **2023,** *7* (7), 887-900.
23. Staufer, O.; Antona, S.; Zhang, D.; Csatari, J.; Schroter, M.; Janiesch, J. W.; Fabritz, S.; Berger, I.; Platzman, I.; Spatz, J. P., Microfluidic production and characterization of biofunctionalized giant unilamellar vesicles for targeted intracellular cargo delivery. *Biomaterials* **2021,** *264*, 120203.
24. Maeki, M.; Kimura, N.; Sato, Y.; Harashima, H.; Tokeshi, M., Advances in microfluidics for lipid nanoparticles and extracellular vesicles and applications in drug delivery systems. *Adv Drug Deliv Rev* **2018,** *128*, 84-100.
25. Gehl, J., Electroporation: theory and methods, perspectives for drug delivery, gene therapy and research. *Acta Physiol Scand* **2003,** *177* (4), 437-47.
26. Bosch, S.; de Beaurepaire, L.; Allard, M.; Mosser, M.; Heichette, C.; Chretien, D.; Jegou, D.; Bach, J. M., Trehalose prevents aggregation of exosomes and cryodamage. *Sci Rep* **2016,** *6*, 36162.
27. Yuan, F.; Li, Y. M.; Wang, Z., Preserving extracellular vesicles for biomedical applications: consideration of storage stability before and after isolation. *Drug Deliv* **2021,** *28* (1), 1501-1509.
28. Johnsen, K. B.; Gudbergsson, J. M.; Skov, M. N.; Christiansen, G.; Gurevich, L.; Moos, T.; Duroux, M., Evaluation of electroporation-induced adverse effects on adipose-derived stem cell exosomes. *Cytotechnology* **2016,** *68* (5), 2125-38.
29. Budgude, P.; Kale, V.; Vaidya, A., Cryopreservation of mesenchymal stromal cell-derived extracellular vesicles using trehalose maintains their ability to expand hematopoietic stem cells in vitro. *Cryobiology* **2021,** *98*, 152-163.
30. Neo, S. H.; Chung, K. Y.; Quek, J. M.; Too, H. P., Trehalose significantly enhances the recovery of serum and serum exosomal miRNA from a paper-based matrix. *Sci Rep* **2017,** *7* (1), 16686.
31. Gorgens, A.; Corso, G.; Hagey, D. W.; Jawad Wiklander, R.; Gustafsson, M. O.; Felldin, U.; Lee, Y.; Bostancioglu, R. B.; Sork, H.; Liang, X.; Zheng, W.; Mohammad, D. K.; van de Wakker, S. I.; Vader, P.; Zickler, A. M.; Mamand, D. R.; Ma, L.; Holme, M. N.; Stevens, M. M.; Wiklander, O. P. B.; El Andaloussi, S., Identification of storage conditions stabilizing extracellular vesicles preparations. *J Extracell Vesicles* **2022,** *11* (6), e12238.
32. Ding, N.; Lee, S.; Lieber-Kotz, M.; Yang, J.; Gao, X., Advances in genome editing for genetic hearing loss. *Adv Drug Deliv Rev* **2020**.
33. Gao, X.; Tao, Y.; Lamas, V.; Huang, M.; Yeh, W. H.; Pan, B.; Hu, Y. J.; Hu, J. H.; Thompson, D. B.; Shu, Y.; Li, Y.; Wang, H.; Yang, S.; Xu, Q.; Polley, D. B.; Liberman, M. C.; Kong, W. J.; Holt, J. R.; Chen, Z. Y.; Liu, D. R., Treatment of autosomal dominant hearing loss by in vivo delivery of genome editing agents. *Nature* **2018,** *553* (7687), 217-221.
34. Zheng, Z.; Li, G.; Cui, C.; Wang, F.; Wang, X.; Xu, Z.; Guo, H.; Chen, Y.; Tang, H.; Wang, D.; Huang, M.; Chen, Z. Y.; Huang, X.; Li, H.; Li, G. L.; Hu, X.; Shu, Y., Preventing autosomal-dominant hearing loss in Bth mice with CRISPR/CasRx-based RNA editing. *Signal Transduct Target Ther* **2022,** *7* (1), 79.
35. Guo, Y.; Han, L.; Han, S.; Tang, H.; Wang, S.; Cui, C.; Chen, B.; Li, H.; Shu, Y., Specific knockdown of Htra2 by CRISPR-CasRx prevents acquired sensorineural hearing loss in mice. *Mol Ther Nucleic Acids* **2022,** *28*, 643-655.
36. Nakanishi, H.; Ohtsubo, M.; Iwasaki, S.; Hotta, Y.; Takizawa, Y.; Hosono, K.; Mizuta, K.; Mineta, H.; Minoshima, S., Mutation analysis of the MYO7A and CDH23 genes in Japanese patients with Usher syndrome type 1. *J Hum Genet* **2010,** *55* (12), 796-800.

37. Sun, Y.; Chen, J.; Sun, H.; Cheng, J.; Li, J.; Lu, Y.; Lu, Y.; Jin, Z.; Zhu, Y.; Ouyang, X.; Yan, D.; Dai, P.; Han, D.; Yang, W.; Wang, R.; Liu, X.; Yuan, H., Novel missense mutations in MYO7A underlying postlingual high- or low-frequency non-syndromic hearing impairment in two large families from China. *J Hum Genet* **2011,** *56* (1), 64-70.
38. VanderBurgh, J. A.; Corso, T. N.; Levy, S. L.; Craighead, H. G., Scalable continuous-flow electroporation platform enabling T cell transfection for cellular therapy manufacturing. *Sci Rep* **2023,** *13* (1), 6857.
39. Zhan, Y.; Wang, J.; Bao, N.; Lu, C., Electroporation of cells in microfluidic droplets. *Anal Chem* **2009,** *81* (5), 2027-31.
40. Hsi, P.; Christianson, R. J.; Dubay, R. A.; Lissandrello, C. A.; Fiering, J.; Balestrini, J. L.; Tandon, V., Acoustophoretic rapid media exchange and continuous-flow electrotransfection of primary human T cells for applications in automated cellular therapy manufacturing. *Lab Chip* **2019,** *19* (18), 2978-2992.
41. Bawazer, L. A.; McNally, C. S.; Empson, C. J.; Marchant, W. J.; Comyn, T. P.; Niu, X.; Cho, S.; McPherson, M. J.; Binks, B. P.; deMello, A.; Meldrum, F. C., Combinatorial microfluidic droplet engineering for biomimetic material synthesis. *Sci Adv* **2016,** *2* (10), e1600567.
42. Prastowo, A.; Feuerborn, A.; Cook, P. R.; Walsh, E. J., Biocompatibility of fluids for multiphase drops-in-drops microfluidics. *Biomed Microdevices* **2016,** *18* (6), 114.
43. Martinon, D.; Borges, V. F.; Gomez, A. C.; Shimada, K., Potential Fast COVID-19 Containment With Trehalose. *Front Immunol* **2020,** *11*, 1623.
44. Sartipzadeh, O.; Naghib, S. M.; Seyfoori, A.; Rahmanian, M.; Fateminia, F. S., Controllable size and form of droplets in microfluidic-assisted devices: Effects of channel geometry and fluid velocity on droplet size. *Mater Sci Eng C Mater Biol Appl* **2020,** *109*, 110606.
45. Self, T.; Mahony, M.; Fleming, J.; Walsh, J.; Brown, S. D.; Steel, K. P., Shaker-1 mutations reveal roles for myosin VIIA in both development and function of cochlear hair cells. *Development* **1998,** *125* (4), 557-66.
46. Sloan-Heggen, C. M.; Bierer, A. O.; Shearer, A. E.; Kolbe, D. L.; Nishimura, C. J.; Frees, K. L.; Ephraim, S. S.; Shibata, S. B.; Booth, K. T.; Campbell, C. A.; Ranum, P. T.; Weaver, A. E.; Black-Ziegelbein, E. A.; Wang, D.; Azaiez, H.; Smith, R. J. H., Comprehensive genetic testing in the clinical evaluation of 1119 patients with hearing loss. *Hum Genet* **2016,** *135* (4), 441-450.
47. Hendel, A.; Bak, R. O.; Clark, J. T.; Kennedy, A. B.; Ryan, D. E.; Roy, S.; Steinfeld, I.; Lunstad, B. D.; Kaiser, R. J.; Wilkens, A. B.; Bacchetta, R.; Tsalenko, A.; Dellinger, D.; Bruhn, L.; Porteus, M. H., Chemically modified guide RNAs enhance CRISPR-Cas genome editing in human primary cells. *Nature Biotechnology* **2015,** *33* (9), 985-989.
48. Huang, T.; Cheng, A. G.; Stupak, H.; Liu, W.; Kim, A.; Staecker, H.; Lefebvre, P. P.; Malgrange, B.; Kopke, R.; Moonen, G.; Van De Water, T. R., Oxidative stress-induced apoptosis of cochlear sensory cells: otoprotective strategies. *Int J Dev Neurosci* **2000,** *18* (2-3), 259-70.
49. Staecker, H.; Zheng, Q. Y.; Van De Water, T. R., Oxidative stress in aging in the C57B16/J mouse cochlea. *Acta Otolaryngol* **2001,** *121* (6), 666-72.
50. Rosazza, C.; Meglic, S. H.; Zumbusch, A.; Rols, M. P.; Miklavcic, D., Gene Electrotransfer: A Mechanistic Perspective. *Curr Gene Ther* **2016,** *16* (2), 98-129.

Acknowledgments:

The authors would like to thank Interdisciplinary Center for Biotechnology Research (ICBR) core facility at the University of Florida, and imaging core facility support from University of Kansas Medical Center. We acknowledge funding supports from NIH 1R35GM133794, CFF HE21I0, and UFHCC GU pilot to Dr Mei He.

Competing interests: Authors declare that they have no competing interests.